

Mechanical control of spin-orbit splitting in GaAs and InGaAs epilayers

V. Sih, H. Knotz, J. Stephens, V. R. Horowitz, A. C. Gossard, and D. D. Awschalom*

*Center for Spintronics and Quantum Computation
University of California, Santa Barbara, CA 93106*

(Dated: May 13, 2018)

Time-resolved Kerr rotation spectroscopy as a function of pump-probe distance, voltage and magnetic field is used to measure the momentum-dependent spin splitting energies in GaAs and InGaAs epilayers. The strain of the samples can be reproducibly controlled in the cryostat using three- and four-point bending applied with a mechanical vise. We find that the magnitude of the spin splitting increases linearly with applied tension and voltage. A strain-drift-diffusion model is used to relate the magnitude of the measured spin-orbit splitting to the amount of strain in the sample.

PACS numbers: 71.70.Ej, 71.70.Fk, 72.25.Dc, 72.25.Rb

Potential applications in spintronics¹ and quantum information processing² rely upon an understanding of the effect of electric fields and strain on electron spins. Strain reduces the symmetry of a crystal, which introduces momentum \mathbf{k} -linear terms to the Dresselhaus³ and Bychkov-Rashba⁴ spin splittings. These strain-induced effective magnetic fields can be used to generate electron spin polarization electrically⁶ and coherently manipulate spins using electric fields and in the absence of magnetic fields⁵, but they also contribute to more efficient spin relaxation⁷. In addition, recent steady-state measurements^{8,9} have shown that the spatial period of strain-induced spin precession is independent of the applied electric field, which demonstrates the robustness of strain-induced spin precession for applications in functional spin-based devices.

Here we employ mechanical three- and four-point bending to tune the tensile strain of GaAs and InGaAs epilayers while performing low-temperature time-resolved magneto-optical spectroscopy to determine the magnitude of the strain-induced spin splitting. The samples are contacted so that an in-plane electric field can be applied to impart an average drift velocity to the optically-excited electron spins. Kerr rotation measurements as a function of magnetic field and pump-probe distance are performed for different applied electric fields, and we observe that the spin splitting increases with increasing drift velocity and tensile strain. Unlike previous measurements that introduced strain through heterostructure engineering and lattice-mismatched growth⁵, these measurements are able to map out the strain dependence in a single sample and without the complications of strain relaxation. The vise geometry allows for repeatable tensioning of samples and precise control over the strain level.

The samples are grown using molecular beam epitaxy on semi-insulating (001) GaAs substrates. We examine both n-doped GaAs and InGaAs epilayers. The GaAs samples are comprised of 100 nm undoped GaAs buffer layer, 400 nm Al_{0.7}Ga_{0.3}As, and a 500 nm Si-doped GaAs epilayer. Samples with carrier densities of $2 \times 10^{16} \text{ cm}^{-3}$ and $4 \times 10^{16} \text{ cm}^{-3}$ were measured, but since they exhibit

qualitatively similar behavior, we show only data for the $2 \times 10^{16} \text{ cm}^{-3}$ n-GaAs sample in this paper. The InGaAs sample is composed of 300 nm of growth-interrupted GaAs buffer layer, 500 nm of Si-doped In_{0.04}Ga_{0.96}As with a carrier concentration of $3 \times 10^{16} \text{ cm}^{-3}$, and 100 nm of undoped GaAs. The lattice constant of the InGaAs layer is matched to that of GaAs, as confirmed using x-ray diffraction. Since InGaAs has a larger natural lattice constant than GaAs, the InGaAs layer is compressively strained in-plane as grown.

The samples are patterned into mesas using photolithography and a chemical wet etch and then contacted using annealed Ni/AuGe [Fig. 1(a)]. The channels have a width $w = 120 \mu\text{m}$ and length $l = 310 \mu\text{m}$ between the contacts and are aligned such that an electric field $E = V/l$ can be applied along either the [110] (x) or [110] (y) directions. The samples are then mounted into either a three- or four-point mechanical bending vise. While the four-point bending geometry produces strain that is uniform between the central two points¹⁰, higher maximum values of strain can be achieved in the three-point geometry before structural failure occurs. In the case of the four-point bending, the mesas are patterned far from the four contact points, minimizing local strain variations. The sample is cooled to a temperature $T = 60 \text{ K}$, at which nuclear polarization is negligible¹¹. For the field-dependent measurements, a magnetic field is applied along x . A cross-section of the measurement geometry is shown in Fig. 1(b). The vise is tightened along the z direction, introducing tensile strain along x . The optical measurements are performed along z and measure the spin polarization along [001].

Time-resolved Kerr rotation spectroscopy¹² is used to monitor the electron spin dynamics in the samples. In this technique, a Ti:Sapphire laser, tuned to the absorption edge of the material that we wish to probe (wavelength $\lambda = 818 \text{ nm}$ for GaAs and $\lambda = 850 \text{ nm}$ for In_{0.04}Ga_{0.96}As), produces a train of $\sim 250 \text{ fs}$ pulses at a repetition rate of 76 MHz, which are split into a pump beam (2 mW) and a probe beam (200 μW) with 30 μm diameters. The pump pulse is circularly-polarized and excites a spin-polarized electron population in the epi-

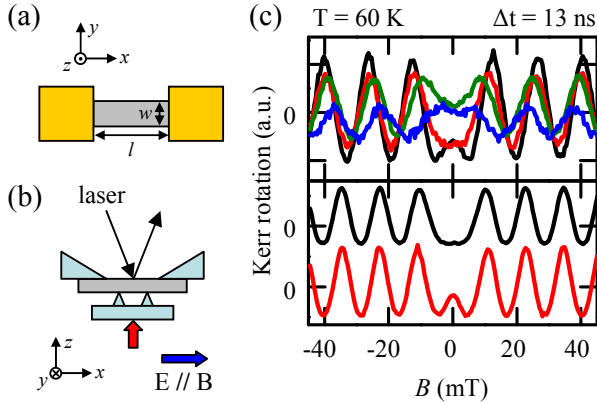


FIG. 1: (a) Patterned sample. Mesa is shown in grey, and metal contacts are shown in gold. (b) Measurement geometry showing orientation of sample, mechanical vise, electric and magnetic fields and optical measurement. (c) (top) Kerr rotation at temperature $T = 60$ K on $2 \times 10^{16} \text{ cm}^{-3}$ GaAs epilayer as a function of applied magnetic field for electric field $E = 32 \text{ V cm}^{-1}$ and pump-probe separation $d = 38 \mu\text{m}$ at time delay $\Delta t = 13$ ns for strained states 2 (black), 3 (red), 4 (green) and 5 (blue). (bottom) Kerr rotation on InGaAs epilayer for unstrained (black) and strained (red) states.

layer. A linearly-polarized probe pulse is incident on the sample at time Δt later, which is controlled using a mechanical delay line. The electron spin polarization in the sample is measured by detecting the change in the polarization axis, or Kerr rotation, of the reflected probe beam. Time-resolved measurements at temperature $T = 60$ K and an applied magnetic field $B = 0.2$ T show that the electron g-factor is -0.43 for the GaAs epilayer and -0.48 for the InGaAs epilayer and that the transverse spin coherence time is 40 ns for GaAs and 3 ns for the InGaAs sample. For the spatially-resolved measurements, a stepper motor-driven mirror changes the spatial separation d between the pump and probe beams¹³. The applied electric field causes the spins to drift with an average velocity v_d and imparts a non-zero average momentum $\langle \mathbf{k} \rangle$ to the electron spin packet.

In order to determine the \mathbf{k} -dependent internal magnetic field B_{int} , we measure Kerr rotation as a function of the applied magnetic field B_{ext} at $\Delta t = 13$ ns for various E and pump-probe distances. The presence of B_{int} modifies the symmetric sinusoidal field-dependent signal^{5,13,14}. When B_{int} is along the same direction as B_{ext} , the signal becomes centered about $-B_{\text{int}}$, but if B_{int} and B_{ext} are perpendicular, as is the case when the electric field and B_{ext} are applied along the same direction, the data can be fit to the equation:

$$\text{KR} = A \cos(g\mu_B \sqrt{B_{\text{ext}}^2 + B_{\text{int}}^2} \Delta t / \hbar) \quad (1)$$

where A is the amplitude, g the effective g-factor of the sample, μ_B the Bohr magneton, and \hbar is Planck's constant over 2π . For $E = 32 \text{ V cm}^{-1}$ and $\Delta t = 13$ ns, the center of the electron spin packet is observed to be

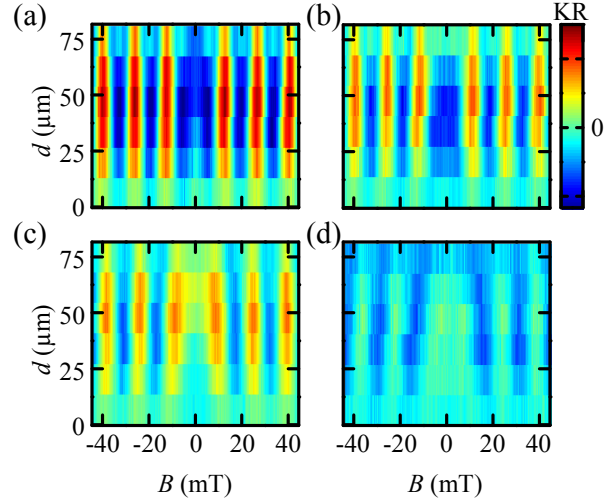


FIG. 2: Kerr rotation at temperature $T = 60$ K and time delay $\Delta t = 13$ ns as a function of applied magnetic field B_{ext} and pump-probe separation d on $2 \times 10^{16} \text{ cm}^{-3}$ GaAs epilayer sample for electric field $E = 32 \text{ V cm}^{-1}$ for (a) strained states 2 (b) 3 (c) 4 and (d) 5. The color scale is the same for all four plots.

at pump-probe separation $d = 38 \mu\text{m}$. Figure 1(c) (top) shows data for the GaAs sample for different amounts of tension applied using the four-point bending vise. We measure Kerr rotation in the channel for the unstrained case and for five increasing levels of strain, which we label as strained states 1 - 5. The vise is tightened by the same amount between each of these strained states. Increasing the strain in the GaAs sample decreases the signal amplitude and increases the spin precession frequency and B_{int} . The change in the amplitude is due to a decrease in the spin lifetime, which we confirm using time-resolved Kerr rotation. In contrast, measurements on InGaAs, shown in Fig. 1(c) (bottom), show that the application of tensile strain via the three-point bending vise leads to some relaxation of the compressive strain due to lattice mismatch. The Kerr rotation amplitude is increased, and B_{int} is decreased. Measurements were also performed on the $2 \times 10^{16} \text{ cm}^{-3}$ GaAs sample for channels where E was applied along y and perpendicular to B_{ext} and the direction of the tensile strain; in this geometry, B_{int} is parallel to B_{ext} , and the values obtained for B_{int} were 22% smaller.

We explore the strain-dependent spin-orbit splitting in the GaAs sample as a function of electric field and pump-probe distance. In Figures 2(a)-(d), we show Kerr rotation as a function of applied magnetic field and pump-probe separation for strained states 2, 3, 4, and 5 for $E = 32 \text{ V cm}^{-1}$ and $\Delta t = 13$ ns. The color scale is the same for all four plots. Again, we observe that the spin precession period and amplitude decrease with strain and that an increase in B_{int} lowers the central peak. In these measurements, we also observe the effect of spin diffusion, which is manifest in the spatial dependence of B_{int} .

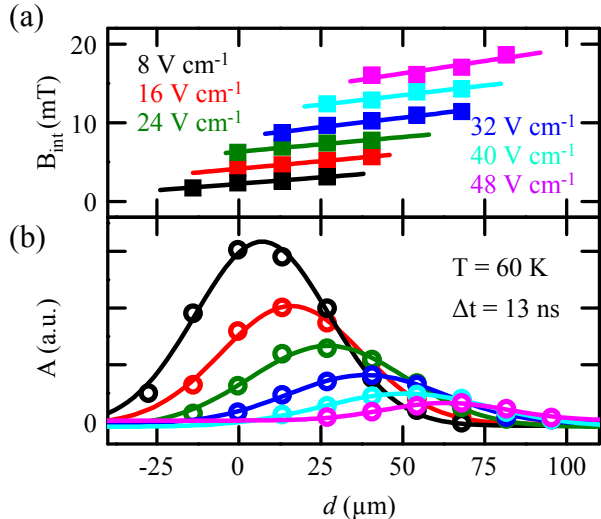


FIG. 3: (a) Effective magnetic field B_{int} and (b) amplitude A as a function of pump-probe separation d on the 2×10^{16} cm⁻³ GaAs epilayer sample in strained state 4 for electric field $E = 8$ (black), 16 (red), 24 (green), 32 (blue), 40 (cyan) and 48 V cm⁻¹ (magenta). Symbols are data, and lines are fits as described in text.

and is due to the spread in drift velocities of the spin packet.

In order to characterize the voltage-dependence of B_{int} , we fit the amplitude A as a function of d with a Gaussian function to determine the center position of the spin packet d_c . We then use the results of a linear fit of B_{int} to determine the value of B_{int} at d_c for each voltage. In Figure 3, we show the data (symbols) and fits (lines) for A and B_{int} for the GaAs sample for strained state 4 as a function of d and for various values of E . From these fits, we obtain the spin-splitting energy $\Delta_0 = g \mu_B B_{\text{int}}$ at the center of the spin packet as a function of v_d , which is plotted in Fig. 4 for increasing amounts of strain in the 2×10^{16} cm⁻³ GaAs sample. As observed previously⁵, the data can be fit to a line, where the slope $\beta = \Delta_0/v_d$ can be used to characterize the observed effect. We plot β for each of the strained states in the inset of Fig. 4 and observe that β increases for increasing amounts of applied tension. In comparison, previous measurements⁵ on GaAs strained by the removal of the underlying substrate showed that $\beta = 99$ neV ns μm⁻¹. Similar measurements of the InGaAs sample reveal that $\beta = 72$ neV ns μm⁻¹ when unstrained and $\beta = 40$ neV ns μm⁻¹ when strained with the three-point bending vise.

Although we tightened the mechanical vise by the same amount between each of the strained states, slip and play in the vise make it difficult to determine the amount of bending and strain in the sample by the mechanical displacement Δz . In order to estimate the amount of strain for each of the strained states, we solve a strain-drift-diffusion model^{8,15} to determine the spatial spin precession period as a function of ε . Although this model was developed for steady-state measurements, as described in

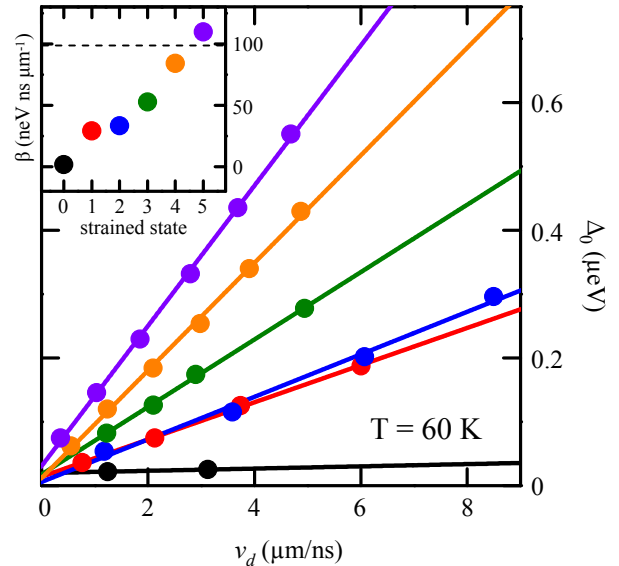


FIG. 4: Spin-splitting energy Δ_0 as a function of drift velocity v_d for 2×10^{16} cm⁻³ GaAs epilayer sample when unstrained (black symbols) and strained states 1 (red), 2 (blue), 3 (green), 4 (orange), and 5 (purple). Linear fits are also shown. (inset) β [neV ns μm⁻¹] for unstrained (0) and strained states 1 - 5. The dashed line indicates β from measurements on a GaAs membrane in Ref. [5].

Ref. [8], using the spatial spin precession period¹⁶ $SPP = 2 \pi \hbar / \beta$, we can relate β and ε . The model parameters used are similar to those used in Ref. [8,15] with the exception of the spin diffusion constant D . A value of $D = 283$ V/cm² was obtained from the measurements in Fig. 3. The strain-drift-diffusion equations are

$$O_1 \rho_x = O_2 \rho_z \quad (2)$$

$$O_1 \rho_y = O_3 \rho_z \quad (3)$$

$$O_4 \rho_z + O_2 \rho_x + O_3 \rho_y = -G_z \quad (4)$$

where the operators O_1 - O_4 are defined as follows,

$$O_1 = D \nabla^2 + \mu \mathbf{E} \cdot \nabla - (C_S D)^2 - \frac{1}{\tau_s} \quad (5)$$

$$O_2 = -C_{B_y} - C_S (2D \frac{\partial}{\partial x} + \mu E_x) \quad (6)$$

$$O_3 = C_{B_x} - C_S (2D \frac{\partial}{\partial y} + \mu E_y) \quad (7)$$

$$O_4 = D \nabla^2 + \mu \mathbf{E} \cdot \nabla - 2(C_S D)^2 - \frac{1}{\tau_s} \quad (8)$$

Here ρ_i is the {x,y,z} component of electron spin polarization, G_z is a Gaussian source function with a FWHM

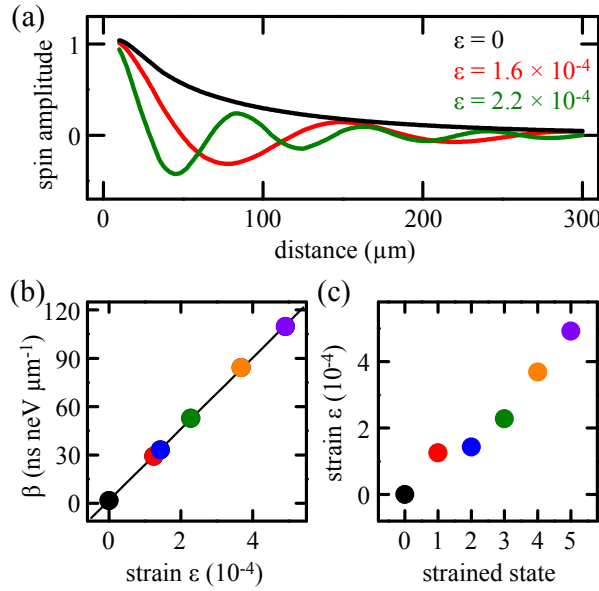


FIG. 5: (a) Spin polarization ρ_z as a function of distance solved using the strain-drift-diffusion model for $\varepsilon = 0$ (black), 1.6 (red) and 2.2×10^{-4} (green). (b) The linear relation between β and strain ε from the strain-drift-diffusion model (line). The symbols show β obtained from measurements on the $2 \times 10^{16} \text{ cm}^{-3}$ GaAs epilayer sample. (c) Estimates of strain ε for the strained states from the measured β .

of $30 \mu\text{m}$, D is the spin diffusion constant, μ is the mobility, τ_s is the spin relaxation time, \mathbf{E} is the applied electric

field, \mathbf{B} is the applied magnetic field, $C_S = C_3 \text{ m}^* \varepsilon / \hbar^2$, $\hbar C_{B_i} = g \mu B_i$, m^* is the electron effective mass, and ε is the strain. We assume a value for the spin-strain coupling coefficient $C_3 = 4.0 \text{ eV } \text{\AA}$, as in Ref. [15]. The equations are solved over a $1 \times 1 \text{ mm}$ field using a finite element method. For the strain calibration, the external applied magnetic field was set to zero, and an electric field of 33 V cm^{-1} was used. We obtain solutions of the spin polarization as a function of position for varying values of ε between 0 and 0.001 . Figure 5(a) shows three line cuts of ρ_z taken along the direction of the electric field for different solutions with $\varepsilon = 0$, 1.6 , and 2.2×10^{-4} . We fit these line cuts to determine the spatial spin precession frequency as a function of ε . A linear fit of β as a function of ε yields a slope of 22.27 ± 0.96 in units of β per 10^{-4} unit strain. Figure 5(b) shows β as a function of ε . This relation allows us to assign strain values to all six tension states using their measured values of β [Fig. 5(c)].

In summary, we have performed quantitative measurements of the spin-splitting energy as a function of voltage and strain on samples mounted in a mechanical vise. Using a strain-drift-diffusion model, we are able to estimate the strain in the devices and calibrate the observed spin-splitting. This spin-splitting can be used to locally and coherently manipulate electron spins and electrically drive spin resonance^{5,17}.

We acknowledge support from AFOSR, DARPA/DMEA, NSF and ONR.

* Electronic address: awsch@physics.ucsb.edu

¹ S. A. Wolf, D. D. Awschalom, R. A. Buhrman, J. M. Daughton, S. von Molnar, M. L. Roukes, A. Y. Chtchelkina, and D. M. Treger, *Science* **294**, 1488 (2001).

² *Semiconductor Spintronics and Quantum Computation, NanoScience and Technology*, edited by D. D. Awschalom, N. Samarth, and D. Loss (Springer-Verlag, New York 2002).

³ G. Dresselhaus, *Phys. Rev.* **100**, 580 (1955).

⁴ Y. A. Bychkov and E. I. Rashba, *J. Phys. C* **17**, 6039 (1984).

⁵ Y. Kato, R. C. Myers, A. C. Gossard and D. D. Awschalom, *Nature* **427**, 50 (2004).

⁶ Y. K. Kato, R. C. Myers, A. C. Gossard and D. D. Awschalom, *Phys. Rev. Lett.* **93**, 176601 (2004).

⁷ H. Knotz, A. W. Holleitner, J. Stephens, R. C. Myers and D. D. Awschalom, *cond-mat/0511562* (2005).

⁸ S. A. Crooker and D. L. Smith, *Phys. Rev. Lett.* **94**, 236601 (2005).

⁹ M. Beck, C. Metzner, S. Malzer and G. H. Dohler, *cond-mat/0504668* (2005).

¹⁰ E. J. Hearn, *Mechanics of Materials* (Butterworth Heinemann, Oxford, 3rd Ed. 1997), Vol. 1 and 2.

¹¹ J. M. Kikkawa and D. D. Awschalom, *Science* **287**, 473 (2000).

¹² S. A. Crooker, D. D. Awschalom, J. J. Baumberg, F. Flack, and N. Samarth, *Phys. Rev. B* **56**, 7574 (1997).

¹³ J. M. Kikkawa and D. D. Awschalom, *Nature* **397**, 139 (1999).

¹⁴ V. K. Kalevich and V. L. Korenev, *JETP Lett.* **52**, 230 (1990).

¹⁵ M. Hruska, S. Kos, S. A. Crooker, A. Saxena and D. L. Smith, *Phys. Rev. B* **73**, 075306 (2006).

¹⁶ Y. K. Kato, R. C. Myers, A. C. Gossard and D. D. Awschalom, *Appl. Phys. Lett.* **87**, 022503 (2005).

¹⁷ E. I. Rashba and Al. L. Efros, *Appl. Phys. Lett.* **83**, 5295 (2003).